



# SDSS J1042-0018: a Broad Line AGN but Misclassified as an H II Galaxy in the BPT Diagram by Flux Ratios of Narrow Emission Lines

Yi Cao, Si-Dan Zhao, Xing-Yu Zhu, Hai-Chao Yu, Yi-Wei Wang, and Xue-Guang Zhang  
School of Physics and Technology, Nanjing Normal University, Nanjing 210023, China; [xgzhang@njnu.edu.cn](mailto:xgzhang@njnu.edu.cn)  
Received 2021 November 28; revised 2022 January 26; accepted 2022 February 10; published 2022 March 17

## Abstract

In this paper, we discuss properties of SDSS J1042-0018 which is a broad line active galactic nucleus (AGN) but misclassified as an H II galaxy in the BPT diagram (SDSS J1042-0018 is called a misclassified broad line AGN). The emission lines around  $H\alpha$  and around  $H\beta$  are well described by different model functions, considering broad Balmer lines to be described by Gaussian or Lorentz functions. Different model functions lead to different determined narrow emission line fluxes, but the different narrow emission line flux ratios lead SDSS J1042-0018 as an H II galaxy in the BPT diagram. In order to explain the unique properties of the misclassified broad line AGN SDSS J1042-0018, two methods are proposed, the star-forming contributions and the compressed narrow emission line regions with high electron densities near to critical densities of forbidden emission lines. Fortunately, the strong star-forming contributions can be preferred in SDSS J1042-0018. The misclassified broad line AGN SDSS J1042-0018, well explained by star-forming contributions, could provide further clues on the applications of BPT diagrams to the normal broad line AGNs.

*Key words:* active galaxies – active galactic nuclei – emission line galaxies – Quasars

## 1. Introduction

SDSS J1042-0018 (=SDSS J104210.03-001814.7) is a common broad line active galactic nucleus (AGN) with apparent broad emission lines, as the spectra shown in Figure 1 from SDSS (Sloan Digital Sky Survey). However, based on flux ratios of narrow emission lines well discussed in Section 2, SDSS J1042-0018 can be well classified as an H II galaxy in the BPT diagram (Baldwin et al. 1981; Kewley et al. 2001; Kauffmann et al. 2003; Kewley et al. 2006, 2013a, 2019; Zhang et al. 2020). Therefore, in this paper, some special properties of SDSS J1042-0018 are studied and discussed.

Under the commonly accepted and well-known constantly being revised Unified Model (Antonucci 1993; Ramos et al. 2011; Netzer 2015; Audibert et al. 2017; Balokovic et al. 2018; Brown et al. 2019; Kuraszkiewicz et al. 2021), Type-1 AGNs (broad line Active Galactic Nuclei) and Type-2 AGNs (narrow line AGNs) having the similar properties of intrinsic broad and narrow emission lines, however, Type-2 AGNs have their central broad line regions (BLRs) with distances of tens to hundreds of light-days (Kaspi et al. 2000, 2005; Bentz et al. 2006, 2009; Denney et al. 2010; Bentz et al. 2013; Fausnaugh et al. 2017) to central black holes (BHs) totally obscured by central dust torus (or other high density dust clouds), leading to no broad emission lines (especially in the optical band) in observed spectra of Type-2 AGNs. Meanwhile, Type-1 AGNs and Type-2 AGNs have the similar properties of narrow emission lines, due to much extended narrow emission line

regions (NLRs) with distances of hundreds to thousands of pcs (parsecs) to central BHs (Zakamska et al. 2003; Fischer et al. 2013; Hainline et al. 2014; Heckman & Best 2014; Fischer et al. 2017; Sun et al. 2017; Zhang & Feng 2017).

For an emission line object, two main methods can be conveniently applied to classify whether the object is an AGN or not. On one hand, a broad line object with clear spectroscopic features of broad emission lines and the strong blue power-law continuum emissions can be directly classified as a Type-1 AGN. On the other hand, for a narrow line object, the well-known BPT diagrams can be conveniently applied to determine which narrow line object is a Type-2 AGN (narrow line AGN) or an H II galaxy by properties of flux ratios of narrow emission lines. Therefore, the flux ratios of narrow emission lines for broad line objects (Type-1 AGN) can also lead to the objects well classified as AGNs in the BPT diagrams. However, there are some special bright Type-1 AGNs (we called them the misclassified AGNs), of which flux ratios of narrow emission lines lead the AGNs lying in the regions for H II galaxies in the BPT diagrams. More recently, Zhang (2022) have reported the well identified quasar SDSS J1451+2709 as a misclassified quasar, due to its misclassification as an H II galaxy in the BPT diagrams through narrow emission line flux ratios, after considering different model functions applied to describe the emission lines. In this paper, the second misclassified broad line AGN SDSS J1042-0018 is reported and discussed.

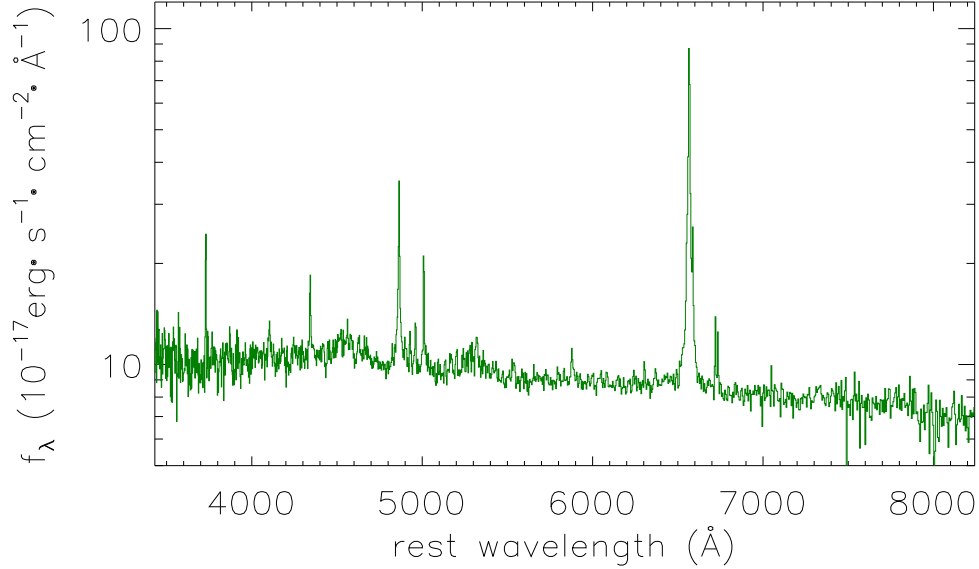


**Figure 1.** The SDSS fiber spectrum of SDSS J1042-0018.

As discussed in Zhang (2022), Type-1 AGNs have more complicated line profiles of emission lines which will be discussed by different model functions leading to quite different properties of narrow emission lines. As the shown results in SDSS J1451+2709 in Zhang (2022), there are intermediate broad emission lines have line width (second moment) around several hundreds of kilometers per second, gently wider than extended components of narrow emission lines, such as the commonly known extended components in [O III] $\lambda$ 4950, 5007  $\text{\AA}$  doublet discussed in Greene & Ho (2005), Shen et al. (2011), Zhang & Feng (2017), Zhang (2021a, 2021b). Once there are multi-epoch spectra, variability properties of emission components can be applied to determine whether one emission component is from NLRs. In this paper, although there is only single-epoch spectrum of SDSS J1042-0018, flux ratios of narrow emission lines can be applied to determine the classifications of SDSS J1042-0018 in the BPT diagram. In this paper, among the SDSS pipeline classified low-redshift quasars ( $z < 0.3$ ) (Richards et al. 2002; Ross et al. 2012), SDSS J1042-0018 is collected as the target, because the SDSS J1042-0018 is the second misclassified broad line AGN as well discussed in the following sections, and further due to its clean line profiles of [O III] doublet without extended components. This paper is organized as follows. Section 2 shows the properties of the spectroscopic emission lines by different model functions with different considerations. Section 3 shows the properties of SDSS J1042-0018 in the BPT diagram. Section 4 discusses the probable physical origin of the unique properties of the misclassified broad line AGN SDSS J1042-0018. Section 5 gives our final summaries and conclusions. Throughout the paper, the cosmological

parameters of  $H_0 = 70 \text{ km s}^{-1} \text{ Mpc}^{-1}$ ,  $\Omega_\Lambda = 0.7$  and  $\Omega_m = 0.3$  have been adopted.

## 2. Properties of Spectroscopic Emission Lines of SDSS J1042-0018

Figure 1 shows the SDSS spectrum of SDSS J1042-0018, with apparent broad emission lines indicating that SDSS J1042-0018 is undoubtedly a broad line AGN (type-1 AGN). In order to show the classification of SDSS J1042-0018 by flux ratios of narrow emission lines in the BPT diagram, the following emission line fitting procedures are applied to describe the emission lines of SDSS J1042-0018, especially the emission lines of narrow H $\beta$ , narrow H $\alpha$ , [O III] $\lambda$ 4959, 5007  $\text{\AA}$  doublet and [N II] $\lambda$ 6548, 6583  $\text{\AA}$  doublet which will be applied in the following BPT diagram, within rest wavelength from 4400 to 5600  $\text{\AA}$  and from 6400 to 6800  $\text{\AA}$ , which are simultaneously fitted by the following two different kinds of model functions. The fitting procedure is very similar to what we have done in Zhang & Feng (2016, 2017), Zhang (2021a, 2021b, 2022), and simply described as follows.

For model A, Gaussian functions are applied to describe the emission lines as follows. Two narrow Gaussian functions are applied to describe the [O III] $\lambda$ 4959, 5007  $\text{\AA}$  doublet. Here, as the following shown best-fitting results, it is not necessary to consider extended components of both [O III] $\lambda$ 4959, 5007  $\text{\AA}$  doublet and the other narrow emission lines. Even two additional Gaussian components were applied to describe the probable extended components of [O III] $\lambda$ 4959, 5007  $\text{\AA}$  doublet and the other narrow emission lines, the determined line fluxes of the extended components near to zero and smaller than determined uncertainties. Therefore, the

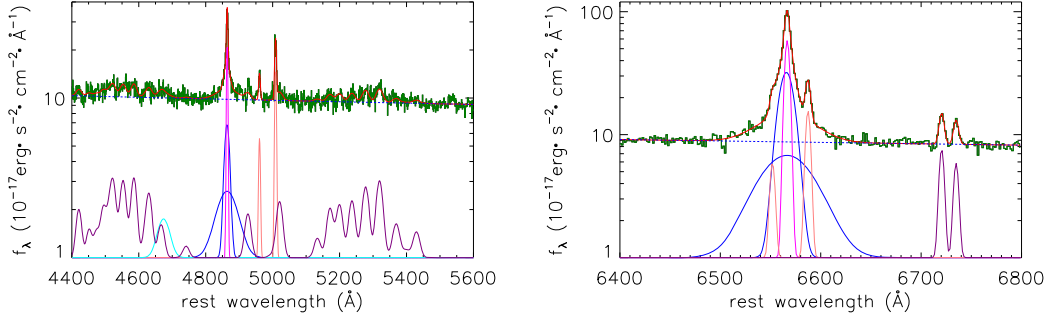


**Figure 2.** The best fitting descriptions to the emission lines around H $\beta$  (left) and H $\alpha$  (right) by multiple Gaussian functions plus power-law continuum emissions. In each panel, the solid dark green line shows the SDSS spectrum, the solid red line shows the determined best-fitting results, the dashed blue line shows the determined power-law continuum emissions. In the left panel, the solid blue lines show the determined broad H $\beta$  described by two broad Gaussian functions, the solid purple line shows the determined optical Fe II emission features, the solid cyan line shows the determined broad He II line, the solid magenta line shows the determined narrow H $\beta$ , the solid pink line shows the determined core components in [O III] doublet. In the right panel, the solid blue lines show the determined two broad components in broad H $\alpha$  described by two broad Gaussian functions, the solid magenta line shows the determined narrow H $\alpha$ , the solid pink lines show the determined [N II] doublet, and the solid purple lines show the determined [S II] doublet. In order to show clear emission features, the Y-axis is in logarithmic coordinate in each panel.

[O III] $\lambda$ 4959, 5007 Å doublet are clear in SDSS J1042-0018. Two narrow Gaussian functions are applied to describe the narrow H $\beta$  and narrow H $\alpha$ . Two<sup>1</sup> broad Gaussian functions are applied to describe the broad H $\beta$ . Two broad Gaussian functions are applied to describe the broad H $\alpha$ . Two<sup>2</sup> narrow Gaussian functions are applied to describe the [S II] $\lambda$ 6716, 6731 Å. One broad Gaussian function is applied to describe the broad He II line. The broadened optical Fe II template in Kovacevic et al. (2010) is applied to describe the optical Fe II emission features. One power law component is applied to describe the AGN continuum emissions underneath the emission lines around H $\beta$ . One power law component is applied to describe the AGN continuum emissions underneath the emission lines around H $\alpha$ . For the model parameters of the model functions in model A, the following restrictions are accepted. First, the flux of each Gaussian component is not smaller than zero. Second, the flux ratio of the [O III] doublet ([N II] doublet) is fixed to the theoretical value 3. Third, the Gaussian components of each forbidden line doublet have the same redshift and the same line width in velocity space. There are no further restrictions on the parameters of Balmer emission lines.

For model B, the model functions are similar to the ones in model A, but the broad H $\beta$  (H $\alpha$ ) is described by one broad Lorentz function. The same restrictions are accepted to the model parameters in model B. The main objective to consider

<sup>1</sup> More than two broad Gaussian functions have also been applied to describe the broad Balmer lines, however, the two or more broad Gaussian components are not necessary, because of the corresponding determined model parameters smaller than their uncertainties.

<sup>2</sup> It is not necessary to consider extended components in [S II] and [N II] doublet. If additional Gaussian components are applied to describe probable extended components in the doublets, the determined line fluxes of the extended components near to zero and smaller than determined uncertainties. Therefore, in this paper, there are no considerations on extended components of the forbidden emission lines.

Lorentz function to describe the broad Balmer lines is as follows. Not similar to Gaussian function, the Lorentz function always has a sharp peak, which can lead to more smaller measured fluxes of narrow Balmer lines, which will have positive effects on the classifications by flux ratios of narrow emission lines in the BPT diagram, which will be discussed in the following section.

Through the Levenberg-Marquardt least-squares minimization technique, the emission lines around H $\beta$  and around H $\alpha$  can be well measured. The best fitting results are shown in Figure 2 with  $\chi^2/\text{dof} = 1.18$  (summed squared residuals divided by degree of freedom) by model functions in model A, and in Figure 3 with  $\chi^2/\text{dof} = 1.19$  by model functions in model B. The line parameters of each Gaussian component of narrow emission lines, Gaussian and Lorentz describe broad Balmer lines, and the power law continuum emissions are listed in Table 1.

The different model functions clearly lead to quite different line parameters of narrow Balmer emission lines (especially line flux of narrow H $\alpha$ ) but similar line parameters of [O III] and [N II] doublets, which will lead to quite different flux ratios of [O III] to narrow H $\beta$  (O3HB) and of [N II] to narrow H $\alpha$  (N2HA).

### 3. SDSS J1042-0018 in the BPT Diagram

#### 3.1. Flux Ratios of Narrow Emission Lines Based on Model A

Based on the measured line parameters listed in Table 1 by model A, the H $\beta_{\text{B1}}$  and H $\alpha_{\text{B1}}$  are certainly from central BLRs, because of their line widths (second moment) quite larger than 900 km s<sup>-1</sup>. The forbidden emission lines are certainly from central NLRs. Comparing with line widths of the [O III] components, the determined narrow components of Balmer

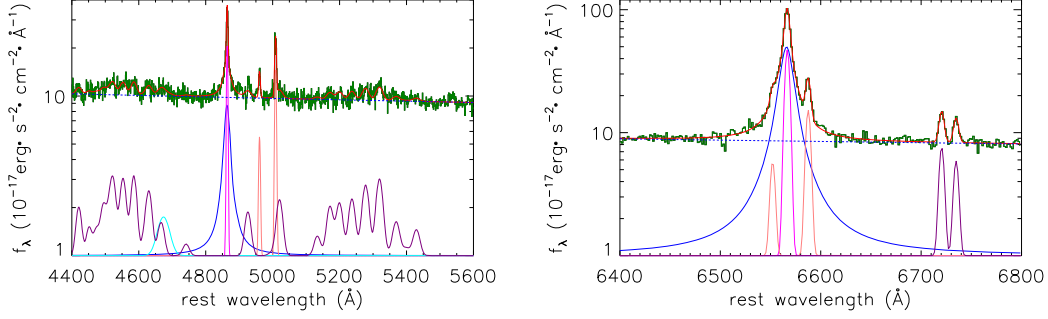


**Figure 3.** Same as Figure 2, but the broad components in Balmer lines are described by Lorentz functions. In each panel, the solid blue line shows the Lorentz-function described broad Balmer line, the other line styles have the same meanings as those in Figure 2.

**Table 1**  
Line parameters of the emission lines

Name	$\lambda_0$	$\sigma$	flux	$\lambda_0$	$\sigma$	flux
Gaussian Broad Balmer lines $\chi^2/\text{dof} = 1.18$			Lorentz Broad Balmer lines $\chi^2/\text{dof} = 1.19$			
$H\beta_{B1}$	$4863.91 \pm 0.78$	$30.29 \pm 4.65$	$121 \pm 16$	$4863.54 \pm 0.42$	$20.28 \pm 2.22$	$247 \pm 11$
$H\beta_{B2}$	$4863.57 \pm 0.09$	$7.51 \pm 0.88$	$109 \pm 13$	...	...	...
He II	$4674.16 \pm 4.88$	$17.63 \pm 4.83$	$34 \pm 8$	$4673.97 \pm 4.78$	$17.04 \pm 4.71$	$32 \pm 8$
$H\beta_N$	$4864.16 \pm 0.04$	$1.99 \pm 0.11$	$99 \pm 8$	$4864.23 \pm 0.05$	$1.98 \pm 0.11$	$98 \pm 8$
[O III] $\lambda$ 5007 Å(N)	$5008.69 \pm 0.18$	$2.48 \pm 0.15$	$85 \pm 6$	$5008.73 \pm 0.18$	$2.44 \pm 0.15$	$83 \pm 6$
$H\alpha_{B1}$	$6566.27 \pm 1.06$	$26.49 \pm 1.24$	$384 \pm 20$	$6565.99 \pm 0.09$	$15.01 \pm 0.66$	$1150 \pm 20$
$H\alpha_{B2}$	$6565.81 \pm 0.12$	$7.38 \pm 0.24$	$575 \pm 19$	...	...	...
$H\alpha_N$	$6566.61 \pm 0.05$	$2.45 \pm 0.08$	$351 \pm 18$	$6566.70 \pm 0.06$	$2.27 \pm 0.11$	$262 \pm 24$
[N II] $\lambda$ 6583 Å	$6587.33 \pm 0.12$	$2.35 \pm 0.12$	$86 \pm 5$	$6587.53 \pm 0.12$	$2.28 \pm 0.11$	$81 \pm 4$
[S II] $\lambda$ 6717 Å	$6720.45 \pm 0.12$	$2.33 \pm 0.13$	$39 \pm 2$	$6720.45 \pm 0.12$	$2.36 \pm 0.12$	$39 \pm 2$
[S II] $\lambda$ 6731 Å	$6734.83 \pm 0.12$	$2.34 \pm 0.13$	$28 \pm 2$	$6734.83 \pm 0.13$	$2.36 \pm 0.13$	$29 \pm 2$
pow $H\beta$	$f_\lambda = (9.57 \pm 0.04) \left(\frac{\lambda}{5100 \text{ \AA}}\right)^{-0.52 \pm 0.05}$			$f_\lambda = (9.57 \pm 0.04) \left(\frac{\lambda}{5100 \text{ \AA}}\right)^{-0.52 \pm 0.05}$		
pow $H\alpha$	$f_\lambda = (8.74 \pm 0.04) \left(\frac{\lambda}{6563 \text{ \AA}}\right)^{-1.74 \pm 0.19}$			$f_\lambda = (8.56 \pm 0.04) \left(\frac{\lambda}{6563 \text{ \AA}}\right)^{-1.59 \pm 0.19}$		

**Note.** The first column shows the information of emission components listed. [O III] $\lambda$ 5007 Å(N) mean the narrow component of [O III] $\lambda$ 5007 Å.  $H\beta_N$  and  $H\alpha_N$  mean the narrow  $H\beta$  and the narrow  $H\alpha$ . The “pow  $H\beta$ ” and the “pow  $H\alpha$ ” mean the power-law continuum emissions around  $H\beta$  and around  $H\alpha$ , respectively. The second column to the fourth column show the line parameters of central wavelength in units of Å, second moment in units of Å and line flux in units of  $10^{-17} \text{ erg s}^{-1} \text{ cm}^{-2}$  of the determined components by Model A with two broad Gaussian functions ( $H\beta_{B1}$ ,  $H\beta_{B2}$  and  $H\alpha_{B1}$ ,  $H\alpha_{B2}$ ) applied to describe the broad Balmer lines. The fifth column to the seventh column show the line parameters of the determined components by Model B with one broad Lorentz function ( $H\beta_{B1}$ ,  $H\alpha_{B1}$ ) applied to describe the broad Balmer lines.

emissions,  $H\beta_N$ , and  $H\alpha_N$ , can be well accepted to come from central NLRs, because their line widths are smaller than the line width of the of [O III] line.

Besides the emission components discussed above, the determined broad component  $H\beta_{B2}$  and  $H\alpha_{B2}$  have line width larger than the line width of [O III] component but smaller than  $900 \text{ km s}^{-1}$ , it is hard to confirm the broad components of  $H\beta_{B2}$  and  $H\alpha_{B2}$  with line width about  $400 \text{ km s}^{-1}$  are from central BLRs.

Finally, for the determined components shown in Figure 2 and with parameters listed in the second column to the fourth column in Table 1, the [N II] and [O III] doublets and narrow

Balmer lines are from central NLRs. Therefore, considering the  $H\beta_{B2}$  and  $H\alpha_{B2}$  coming from central NLRs, the lower limit of flux ratio of [O III] $\lambda$ 5007 Å to narrow  $H\beta$  (including two components of  $H\beta_N$  and  $H\beta_{B2}$ ) and lower limit of flux ratio of [N II] $\lambda$ 6583 Å to narrow  $H\alpha$  (including two components of  $H\alpha_N$  and  $H\alpha_{B2}$ ) can be estimated as

$$\begin{aligned}
 \text{O3HB}_{\text{LA}} &= \frac{f_{[\text{O III}]\lambda 5007 \text{ \AA(N)}}}{f_{H\beta_N} + f_{H\beta_{B2}}} = 0.41 \pm 0.04; \\
 \text{N2HA}_{\text{LA}} &= \frac{f_{[\text{N II}]\lambda 6583 \text{ \AA}}}{f_{H\alpha_N} + f_{H\alpha_{B2}}} = 0.093 \pm 0.004 \quad (1)
 \end{aligned}$$

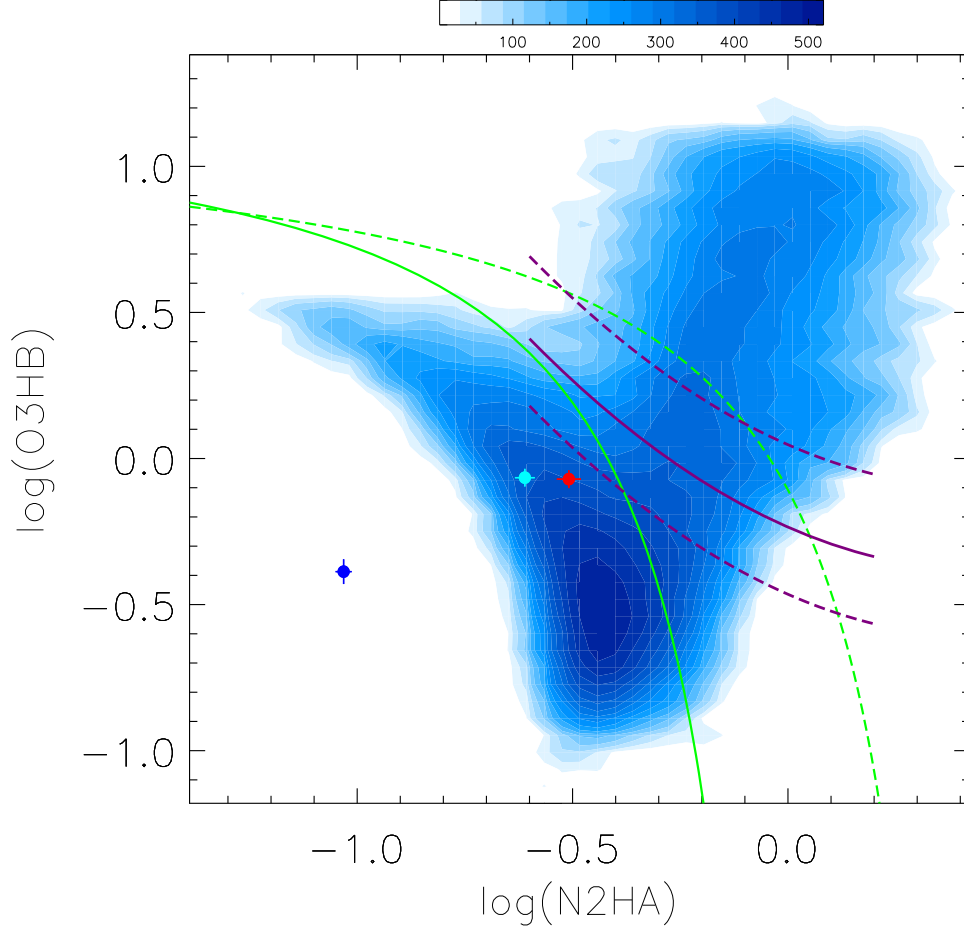


**Figure 4.** The BPT diagram for more than 35,000 narrow line objects (contour in bluish colors) and the misclassified broad line AGN SDSS J1042-0018 (solid circles in red, cyan, purple) by O3HB versus N2HA. Solid and dashed green lines show the dividing lines reported in Kauffmann et al. (2003) and in Kewley et al. (2001) between H II galaxies, composite galaxies and AGNs. The solid purple line and dashed purple lines show the dividing line between H II galaxies and AGNs and the area for composite galaxies determined in our recent work in Zhang et al. (2020) to determine the dividing lines in the BPT diagram through the powerful t-SNE technique. The contour is created by emission line properties of more than 35,000 narrow emission-line galaxies discussed in Zhang et al. (2020) collected from SDSS DR15. Corresponding number densities to different colors are shown in the color bar. Solid circles in blue, cyan and red represent the results of  $[N2HA_{LA}, O3HB_{LA}]$ ,  $[N2HA_{UA}, O3HB_{UA}]$  and  $[N2HA_B, O3HB_B]$ , respectively.

If considering the  $H\beta_{B2}$  and  $H\alpha_{B2}$  coming from central BLRs, the upper limit of flux ratio of  $[O III]\lambda 5007 \text{ \AA}$  to narrow  $H\beta$  (only one component  $H\beta_N$ ) and the upper limit of flux ratio of  $[N II]\lambda 6583 \text{ \AA}$  to narrow  $H\alpha$  (only one component  $H\alpha_N$ ) can be estimated as

$$\begin{aligned} O3HB_{UA} &= \frac{f_{[O III]\lambda 5007 \text{ \AA}(N)}}{f_{H\beta_N}} = 0.86 \pm 0.06; \\ N2HA_{UA} &= \frac{f_{[N II]\lambda 6583 \text{ \AA}}}{f_{H\alpha_N}} = 0.245 \pm 0.013 \end{aligned} \quad (2)$$

Based on the determined narrow emission line ratios by model A, SDSS J1042-0018 can be plotted in the BPT diagram of O3HB versus N2HA in Figure 4. Considering the dividing lines in the BPT diagram as well discussed in

Kauffmann et al. (2003), Kewley et al. (2006, 2019), Zhang et al. (2020), either  $[N2HA_{UA}, O3HB_{UA}]$  or  $[N2HA_{LA}, O3HB_{LA}]$  applied in the BPT diagram, the SDSS J1042-0018 can be well classified as an H II galaxy with few contributions of central AGN activities, through the properties of narrow emission lines.

### 3.2. Flux Ratios of Narrow Emission Lines Based on Model B

For the results by model B, the determined  $H\beta_{B1}$  and  $H\alpha_{B1}$  have line widths quite larger than  $900 \text{ km s}^{-1}$ , therefore, the determined  $H\beta_{B1}$  and  $H\alpha_{B1}$  can be safely accepted to be from central BLRs. Certainly, the forbidden narrow lines are considered and well accepted from the central NLRs. Then, comparing with the line width  $150 \text{ km s}^{-1}$  of  $[O III]\lambda 5007 \text{ \AA}$ ,

the determined components of narrow emission lines with line widths smaller than  $150 \text{ km s}^{-1}$  can be safely accepted to be from central NLRs.

Finally, for the determined components shown in Figure 3 and with parameters listed in the fifth column to the seventh column in Table 1, the broad components  $H\beta_{B1}$ ,  $H\alpha_{B1}$  are truly from central BLRs, the [N II] and [O III] doublets and narrow Balmer lines are from central NLRs. Therefore, the flux ratio of [O III] $\lambda 5007 \text{ \AA}$  to narrow  $H\beta$  can be estimated as

$$\begin{aligned} \text{O3HB}_B &= \frac{f_{[\text{O III}]\lambda 5007 \text{ \AA}}(N)}{f_{H\beta_N}} = 0.85 \pm 0.06; \\ \text{N2HA}_B &= \frac{f_{[\text{N II}]\lambda 6583 \text{ \AA}}}{f_{H\alpha_N}} = 0.31 \pm 0.02 \end{aligned} \quad (3)$$

Based on model B, SDSS J1042-0018 can be re-plotted in the BPT diagram of O3HB versus N2HA in Figure 4. SDSS J1042-0018 can be well classified as an H II galaxy with few contributions of central AGN activities, through the properties of narrow emission lines.

Finally, based on different model functions to describe emission lines and based on different considerations of emission components from central NLRs, SDSS J1042-0018 can be well classified as an H II galaxy with few contributions of central AGN activities. In this paper, SDSS J1042-0018 can be called a misclassified broad line AGN, based on the applications of the BPT diagram.

#### 4. Physical Origin of the Misclassified Broad Line AGN SDSS J1042-0018?

In order to explain the misclassified broad line AGN SDSS J1042-0018, two reasonable methods can be mainly considered in the section, as what we have discussed in SDSS J1451+2709 in Zhang (2022). On one hand, there is one mechanism leading to stronger narrow Balmer emissions, such as the strong star-forming contributions. On the other hand, there is one mechanism leading to weaker forbidden emission lines, such as the expected high electron densities in central NLRs.

##### 4.1. Strong Star-forming Contributions?

In the subsection, star-forming contributions are checked, in order to explain the quite small value of O3HB, because of stronger star-forming contributions leading to stronger narrow Balmer emission lines. In other words, there are two kinds of flux components included in the narrow Balmer lines and [O III] $\lambda 5007 \text{ \AA}$  and [N II] $\lambda 6583 \text{ \AA}$ , one kind of flux depending on central AGN activities:  $f_{[\text{O III}]}(\text{AGN})$ ,  $f_{[\text{N II}]}(\text{AGN})$ ,  $f_{H\alpha}(\text{AGN})$  and  $f_{H\beta}(\text{AGN})$ , the other kind of flux depending on star-forming:  $f_{[\text{O III}]}(\text{SF})$ ,  $f_{[\text{N II}]}(\text{SF})$ ,  $f_{H\alpha}(\text{SF})$  and  $f_{H\beta}(\text{SF})$ . Then, the measured flux ratio O3HB and N2HA, and the flux ratios O3HB(AGN) and N2HA(AGN) depending on central AGN activities, and the flux ratios O3HB(SF) and N2HA(SF)

depending on star-forming, can be described as

$$\begin{aligned} \text{O3HB} &= \frac{f_{[\text{O III}]}(\text{AGN}) + f_{[\text{O III}]}(\text{SF})}{f_{H\beta}(\text{AGN}) + f_{H\beta}(\text{SF})} \\ \text{N2HA} &= \frac{f_{[\text{N II}]}(\text{AGN}) + f_{[\text{N II}]}(\text{SF})}{f_{H\alpha}(\text{AGN}) + f_{H\alpha}(\text{SF})} \\ \text{O3HB(AGN)} &= \frac{f_{[\text{O III}]}(\text{AGN})}{f_{H\beta}(\text{AGN})} \\ \text{O3HB(SF)} &= \frac{f_{[\text{O III}]}(\text{SF})}{f_{H\beta}(\text{SF})} \\ \text{N2HA(AGN)} &= \frac{f_{[\text{N II}]}(\text{AGN})}{f_{H\alpha}(\text{AGN})} \\ \text{N2HA(SF)} &= \frac{f_{[\text{N II}]}(\text{SF})}{f_{H\alpha}(\text{SF})} \\ f_{[\text{O III}]} &= f_{[\text{O III}]}(\text{AGN}) + f_{[\text{O III}]}(\text{SF}) \\ f_{[\text{N II}]} &= f_{[\text{N II}]}(\text{AGN}) + f_{[\text{N II}]}(\text{SF}) \\ f_{H\beta} &= f_{H\beta}(\text{AGN}) + f_{H\beta}(\text{SF}) \\ f_{H\alpha} &= f_{H\alpha}(\text{AGN}) + f_{H\alpha}(\text{SF}) \end{aligned} \quad (4)$$

where  $f_{[\text{O III}]}$ ,  $f_{[\text{N II}]}$ ,  $f_{H\alpha}$  and  $f_{H\beta}$  mean the measured total line fluxes of [O III] $\lambda 5007 \text{ \AA}$ , [N II] $\lambda 6583 \text{ \AA}$  and narrow Balmer lines.

Based on the three measured data points shown in Figure 4 and the corresponding measured total line fluxes  $f_{[\text{O III}]}$ ,  $f_{[\text{N II}]}$ ,  $f_{H\alpha}$  and  $f_{H\beta}$  listed in Table 1 and discussed in Section 3, expected properties of star-forming contributions  $R_{SF} = f_{H\alpha}(\text{SF})/f_{H\alpha}$  can be simply determined, through the following limitations. First, the determined flux ratios of O3HB(AGN) and N2HA(AGN) clearly lead the data points classified as AGN in the BPT diagram, the data points lying above the dividing line shown as the solid green line in Figure 4. Second, the determined flux ratios of O3HB(SF) and N2HA(SF) clearly lead the data points classified as AGN in the BPT diagram, the data points lying below the dividing line shown as the solid green line in Figure 4. Third, the ratios of  $f_{H\alpha}(\text{SF})$  to  $f_{H\alpha}(\text{AGN})$  are similar to the ratios of  $f_{H\beta}(\text{SF})$  to  $f_{H\beta}(\text{AGN})$ .

Based on model A with considering  $H\beta_{B2}$  and  $H\alpha_{B2}$  from NLRs, the narrow emission line fluxes are about  $f_{[\text{O III}]} \sim 85$ ,  $f_{[\text{N II}]} \sim 86$ ,  $f_{H\alpha} \sim 926$  and  $f_{H\beta} \sim 208$  in the units of  $10^{-17} \text{ erg s}^{-1} \text{ cm}^{-2}$ . Model simulating results can be simply done by the following three steps. First and foremost, based on the measured values of  $f_{[\text{O III}]}$ ,  $f_{[\text{N II}]}$ ,  $f_{H\alpha}$  and  $f_{H\beta}$ , value of  $f_{[\text{O III}]}(\text{AGN})$  can be randomly selected from 0 to 85, leading to the fixed  $f_{[\text{O III}]}(\text{SF}) = 85 - f_{[\text{O III}]}(\text{AGN})$ ; the value of  $f_{[\text{N II}]}(\text{AGN})$  can be randomly selected from 0 to 86, leading to the fixed  $f_{[\text{N II}]}(\text{SF}) = 86 - f_{[\text{N II}]}(\text{AGN})$ ; the value of  $f_{H\alpha}(\text{AGN})$  can be randomly selected from 0 to 926, leading to the fixed  $f_{H\alpha}(\text{SF}) = 926 - f_{H\alpha}(\text{AGN})$  and leading to the

values of  $f_{\text{H}\beta}(\text{AGN})$  and  $f_{\text{H}\beta}(\text{SF})$  determined by

$$\begin{aligned} f_{\text{H}\beta}(\text{AGN}) + f_{\text{H}\beta}(\text{SF}) &= 208 \\ f_{\text{H}\beta}(\text{AGN}) &= \frac{f_{\text{H}\alpha}(\text{AGN})}{f_{\text{H}\alpha}(\text{SF})} \times f_{\text{H}\beta}(\text{SF}) \end{aligned} \quad (5)$$

Besides, based on the randomly selected values of  $f_{[\text{O III}]}(\text{AGN})$ ,  $f_{[\text{N II}]}(\text{AGN})$ ,  $f_{\text{H}\alpha}(\text{AGN})$  and  $f_{\text{H}\beta}(\text{AGN})$ , to determine whether the ratios of  $\text{O3HB}_s = \frac{f_{[\text{O III}]}(\text{AGN})}{f_{\text{H}\beta}(\text{AGN})}$  and  $\text{N2HA}_s = \frac{f_{[\text{N II}]}(\text{AGN})}{f_{\text{H}\alpha}(\text{AGN})}$  can lead to the data point  $[\text{O3HB}_s, \text{N2HA}_s]$  lying above the dividing line shown as the solid green line in the BPT diagram of O3HB versus N2HA. Only if the data point  $[\text{O3HB}_s, \text{N2HA}_s]$  lies in the AGN region in the BPT diagram, the randomly selected values of  $f_{[\text{O III}]}(\text{AGN})$ ,  $f_{[\text{N II}]}(\text{AGN})$ ,  $f_{\text{H}\alpha}(\text{AGN})$  are appropriate values. Therefore, the randomly selected values each time are not always appropriate values. Last but not the least, after the first and the second steps are repeated tens of thousands of times, 5000 appropriate values can be collected for the  $f_{[\text{O III}]}(\text{AGN})$ ,  $f_{[\text{N II}]}(\text{AGN})$ , and  $f_{\text{H}\alpha}(\text{AGN})$ . Then, based on the results through model A with considering  $\text{H}\beta_{\text{B2}}$  and  $\text{H}\alpha_{\text{B2}}$  from NLRs, among 66,000 randomly selected values of  $f_{[\text{O III}]}(\text{AGN})$  from 0 to 85, of  $f_{[\text{N II}]}(\text{AGN})$  from 0 to 86 and of  $f_{\text{H}\alpha}(\text{AGN})$  from 0 to 926, there are 5000 couple data points of  $[\text{O3HB}(\text{AGN}), \text{N2HA}(\text{AGN})]$  classified as AGN, and corresponding 5000 couple data points of  $[\text{O3HB}(\text{SF}), \text{N2HA}(\text{SF})]$  classified as H II, in the BPT diagram of O3HB versus N2HA, shown in the left panel of Figure 5. The top right panel of Figure 5 shows the dependence of  $R_{\text{SF}}(\text{AL})$  on  $\text{N2HA}(\text{SF})(\text{AL})$ , with the determined minimum value 76% of the  $R_{\text{SF}}(\text{AL})$ .

Similarly, based on model A with considering  $\text{H}\beta_{\text{B2}}$  and  $\text{H}\alpha_{\text{B2}}$  from BLRs, the narrow emission line fluxes are about  $f_{[\text{O III}]} \sim 85$ ,  $f_{[\text{N II}]} \sim 86$ ,  $f_{\text{H}\alpha} \sim 351$  and  $f_{\text{H}\beta} \sim 99$  in the units of  $10^{-17} \text{erg s}^{-1} \text{cm}^{-2}$ . Then, among 22,000 randomly selected values of  $f_{[\text{O III}]}(\text{AGN})$ , of  $f_{[\text{N II}]}(\text{AGN})$  and of  $f_{\text{H}\alpha}(\text{AGN})$ , there are 5000 couple data points of  $[\text{O3HB}(\text{AGN}), \text{N2HA}(\text{AGN})]$  classified as AGN, and corresponding 5000 couple data points of  $[\text{O3HB}(\text{SF}), \text{N2HA}(\text{SF})]$  classified as H II, in the BPT diagram of O3HB versus N2HA. Here, we do not show the results in the BPT diagram, which are totally similar as the those shown in the left panel of Figure 5. And the middle right panel of Figure 5 shows the dependence of  $R_{\text{SF}}(\text{AU})$  on  $\text{N2HA}(\text{SF})(\text{AU})$ , with the determined minimum value 37% of  $R_{\text{SF}}(\text{AU})$ .

Based on model B, the narrow emission line fluxes are about  $f_{[\text{O III}]} \sim 83$ ,  $f_{[\text{N II}]} \sim 81$ ,  $f_{\text{H}\alpha} \sim 262$  and  $f_{\text{H}\beta} \sim 98$  in the units of  $10^{-17} \text{erg s}^{-1} \text{cm}^{-2}$ . Then, among 15,000 randomly selected values of  $f_{[\text{O III}]}(\text{AGN})$ , of  $f_{[\text{N II}]}(\text{AGN})$  and of  $f_{\text{H}\alpha}(\text{AGN})$ , there are 5000 couple data points of  $[\text{O3HB}(\text{AGN}), \text{N2HA}(\text{AGN})]$  classified as AGN, and corresponding 5000 couple data points of  $[\text{O3HB}(\text{SF}), \text{N2HA}(\text{SF})]$  classified as H II, in the BPT diagram of O3HB versus N2HA. Here, we do not show the results in the BPT diagram, which are totally similar to those shown in the left panel of Figure 5. The bottom right panel of

Figure 5 shows the dependence of  $R_{\text{SF}}(\text{B})$  on  $\text{N2HA}(\text{SF})(\text{B})$ , with the determined minimum value 22% of  $R_{\text{SF}}(\text{B})$ .

Therefore, the determined star-forming contributions  $R_{\text{SF}}$  should be larger than 22%. The strong star-forming contributions indicate there should be apparent absorption features from the host galaxy in the spectrum of SDSS J1042-0018. Figure 6 shows one composite spectrum created by 0.8 times of the SDSS spectrum of SDSS J1042-0018 plus a mean H II galaxy with continuum intensity at  $5100 \text{ \AA}$  about 0.2 times of the continuum intensity at  $5100 \text{ \AA}$  of the SDSS spectrum of SDSS J1042-0018. Here, the mean spectrum of H II galaxies are created by the large sample of 1298 H II galaxies with signal-to-noise larger than 30 in SDSS DR12. There should be absorption features around  $4000 \text{ \AA}$ , clearly indicating that the star-forming contributions could be well applied to explain the unique properties of the misclassified broad line AGN SDSS J1042-0018.

Before the end of the subsection, there is one point that we should note. As discussed in Kauffmann & Heckman (2009) for galaxies around the boundary as defined in Kauffmann et al. (2003), contributions to  $[\text{O III}]$  emissions by star formations are predicted to be typically 40%–50%, which are roughly agreement with our determined  $R_{\text{SF}}$  with minimum value of about 22% and with maximum value of about 76%, providing further clues to support the star-forming contributions to explain the unique properties of the misclassified broad line AGN SDSS J1042-0018. However, one probable question is proposed why we did not see apparent contribution of AGN activities to the narrow emission lines in SDSS J1042-0018? Actually, as the results shown in Figure 5 for the simulating results, the separated appropriate contributions of AGN activities to narrow emission lines,  $f_{[\text{O III}]}(\text{AGN})$ ,  $f_{[\text{N II}]}(\text{AGN})$ ,  $f_{\text{H}\alpha}(\text{AGN})$ , are randomly determined and lead to the data points on AGN activities apparently lying in the AGN region in the BPT diagram. Therefore, SDSS J1042-0018 including AGN activities but lying in the H II region in the BPT diagram is mainly due to mixed contributions of star formations and AGN activities, if considering star-forming contributions as the preferred model to explain the unique properties of the misclassified broad line AGN SDSS J1042-0018. Moreover, as the shown results in Figure 5, there could be dozens of broad line quasars (a sample of tens of misclassified quasars will be reported and discussed in one of our being prepared manuscripts) lying in the H II regions in the BPT diagrams with applications of narrow emission line properties. Certainly, intrinsic physical origin of the misclassification in BPT diagram is still uncertain, further efforts are necessary.

#### 4.2. Compressed Central NLRs?

Besides the star-forming contributions, high electron density in NLRs can be also applied to explain the unique properties of the misclassified broad line AGN SDSS J1042-0018, because the high electron density near to the critical electron densities

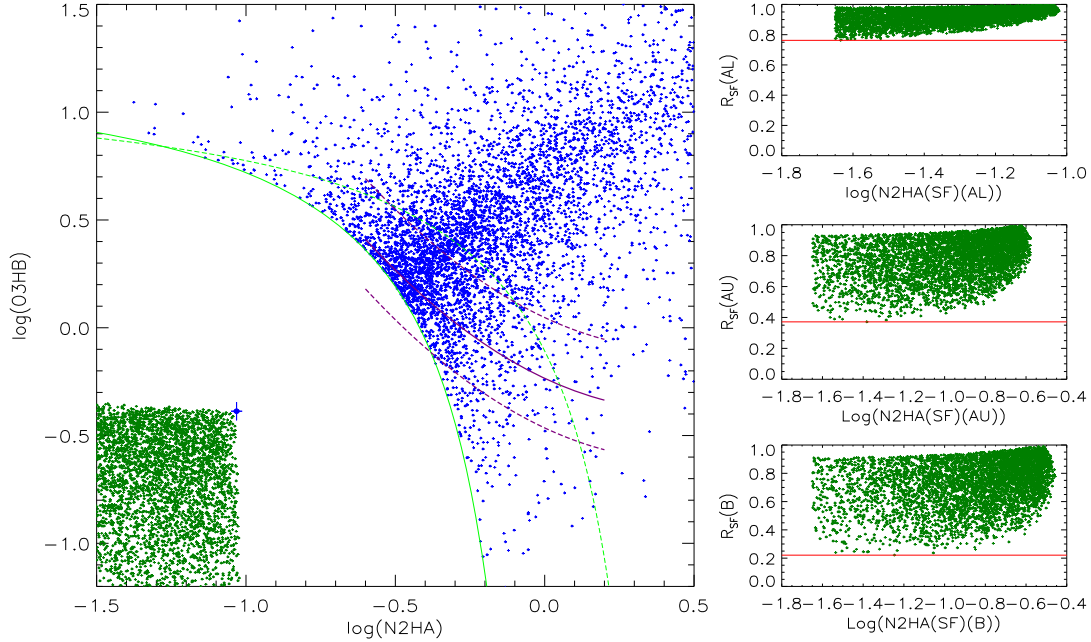


**Figure 5.** Left panel shows the simulated 5000 couple data points of  $[O3HB(AGN), N2HA(AGN)]$  classified as AGN shown as blue pluses, and the simulated 5000 couple data points of  $[O3HB(SF), N2HA(SF)]$  classified as H II shown as dark green pluses, in the BPT diagram of O3HB versus N2HA, based on the narrow line fluxes determined by model A with considering  $H\beta_{B2}$  and  $H\alpha_{B2}$  from central NLRs. The solid blue circle plus error bars and the line styles are the same as those shown in Figure 4. The top right panel shows the dependence of  $R_{SF}(AL)$  on  $N2HA(SF)(AL)$ , based on the narrow line fluxes determined by model A with considering  $H\beta_{B2}$  and  $H\alpha_{B2}$  from central NLRs. The middle right panel shows the dependence of  $R_{SF}(AU)$  on  $N2HA(SF)(AU)$ , based on the narrow line fluxes determined by model A with considering  $H\beta_{B2}$  and  $H\alpha_{B2}$  from central BLRs. The bottom right panel shows the dependence of  $R_{SF}(B)$  on  $N2HA(SF)(B)$ , based on the narrow line fluxes determined by model B. In each right panel, horizontal red line shows the position of the minimum value of  $R_{SF}$ .

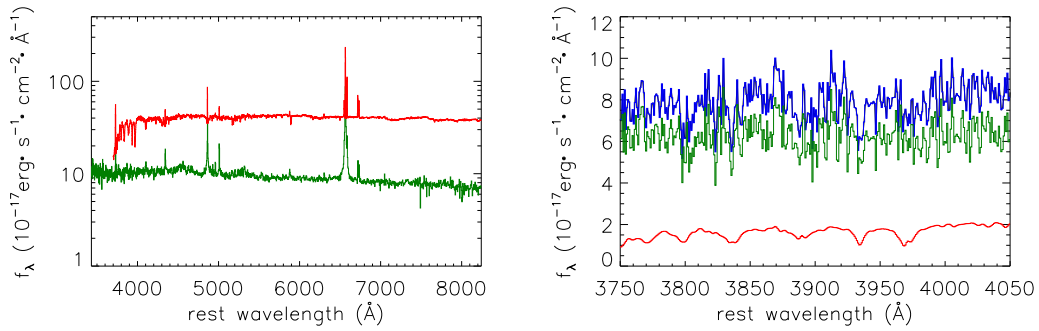


**Figure 6.** Left panel shows the SDSS spectrum of SDSS J1042-0018 in dark green and the mean spectrum of H II galaxies in red. The right panel shows the composite spectrum around 4000 Å, including 20% star-forming contributions. In the right panel, the solid blue line shows the composite spectrum, the solid dark green line shows the SDSS spectrum, and the solid red line shows the star-forming contributions.

of the forbidden emission lines can lead to suppressed line intensities of forbidden emission lines but positive effects on strengthened Balmer emission lines.

It is not hard to determine electron density in NLRs, such as through the flux ratios of  $[S II]\lambda 6717, 6731$  Å doublet as well discussed in Proxauf et al. (2014), Sanders et al. (2016), Kewley et al. (2019). Based on the measured line fluxes of  $[S II]$  doublet listed in Table 1, the flux ratio of  $[S II]\lambda 6716$  Å to  $[S II]\lambda 6731$  Å lead the electron density to be estimated around

$200 \text{ cm}^{-3}$ , a quite normal value, quite smaller than the critical densities around  $10^5 \text{ cm}^{-3}$  to  $[O III]$  and  $[N II]$  doublet.

## 5. Summaries and Conclusions

Finally, we give our summaries and conclusions as follows.

1. Emission lines of the blue quasar SDSS J1042-0018 can be well measured by two different models, broad Balmer lines described by mode A with broad Gaussian functions

and by model B with broad Lorentz functions, leading to different flux ratios of narrow emission lines.

2. Different flux ratios of narrow emission lines determined by different model functions and with different considerations, SDSS J1042-0018 can be well classified as an H II galaxy in the BPT diagram (a misclassified broad line AGN), although the SDSS J1042-0018 actually is a normal broad line AGN.
3. Two reasonable methods are proposed to explain the unique properties of the misclassified broad line AGN SDSS J1042-0018, strong star-forming contributions leading to stronger narrow Balmer emissions, and compressed NLRs with high electron densities leading to suppressed forbidden emissions.
4. Once considering the star-forming contributions, at least 20% star-forming contributions should be preferred in the misclassified broad line AGN SDSS J1042-0018, which will lead to apparent absorption features around 4000 Å, indicating strong star-forming contributions should be preferred in the misclassified broad line AGN SDSS J1042-0018.
5. Once considering the compressed NLRs with high electron densities, the expected electron densities should be around  $10^5 \text{ cm}^{-3}$ . However, the estimated electron density is only around  $200 \text{ cm}^{-3}$  based on the flux ratio of  $[\text{S II}]\lambda 6716 \text{ \AA}$  to  $[\text{S II}]\lambda 6731 \text{ \AA}$ . Therefore, the compressed NLRs with high electron densities are not preferred in the misclassified broad line AGN SDSS J1042-0018.
6. The reported second misclassified broad line AGN SDSS J1042-0018 strongly indicate that there should be extremely unique properties of SDSS J1042-0018 which are currently not detected, or indicate that there should be a small sample of misclassified broad line AGNs similar to SDSS J1042-0018.
7. Narrow emission line properties should be carefully determined in Type-1 AGNs.

### Acknowledgments

We gratefully acknowledge the anonymous referee for giving us constructive comments and suggestions to greatly improve our paper. X.G. Zhang gratefully acknowledges the kind support of Starting Research Fund of Nanjing Normal University, and the kind support of NSFC-12173020. Y. Cao, S.D. Zhao, X.Y. Zhu, H.C. Yu and Y.W. Wang gratefully

acknowledge the kind support of DaChuang project of Nanjing Normal University for undergraduate students. This manuscript has made use of the data from the SDSS projects. The SDSS-III website is <http://www.sdss3.org/>. SDSS-III is managed by the Astrophysical Research Consortium for the Participating Institutions of the SDSS-III Collaborations.

### References

- Antonucci, R. 1993, *ARA&A*, **31**, 473
- Audibert, A., Riffel, R., Sales, D. A., Pastoriza, M. G., & Ruschel-Dutra, D. 2017, *MNRAS*, **464**, 2139
- Baldwin, J. A., Phillips, M., & Terlevich, R. 1981, *PASP*, **93**, 5
- Balokovic, M., Brightman, M., Harrison, F. A., et al. 2018, *ApJ*, **854**, 42
- Bentz, M. C., Peterson, B. M., Netzer, H., Pogge, R. W., & Vestergaard, M. 2009, *ApJ*, **697**, 160
- Bentz, M. C., Peterson, B. M., Pogge, R. W., Vestergaard, M., & Onken, C. A. 2006, *ApJ*, **644**, 133
- Bentz, M. C., Denney, K. D., Grier, C. J., et al. 2013, *ApJ*, **767**, 149
- Brown, A., Nayyeri, H., Cooray, A., et al. 2019, *ApJ*, **871**, 87
- Denney, K. D., Peterson, B. M., Pogge, R. W., et al. 2010, *ApJ*, **721**, 715
- Fausnaugh, M. M., Grier, C. J., Bentz, M. C., et al. 2017, *ApJ*, **840**, 97
- Fischer, T. C., Crenshaw, D. M., Kraemer, S. B., & Schmitt, H. R. 2013, *ApJS*, **209**, 1
- Fischer, T. C., Machuca, C., Diniz, M. R., et al. 2017, *ApJ*, **834**, 30
- Greene, J. E., & Ho, L. C. 2005, *ApJ*, **627**, 721
- Hainline, K. N., Hickox, R. C., Greene, J. E., et al. 2014, *ApJ*, **787**, 65
- Heckman, T. M., & Best, P. N. 2014, *ARA&A*, **52**, 589
- Kaspi, S., Smith, P. S., Netzer, H., et al. 2000, *ApJ*, **533**, 631
- Kaspi, S., Maoz, D., Netzer, H., Peterson, B. M., Vestergaard, M., & Jannuzi, B. T. 2005, *ApJ*, **629**, 61
- Kauffmann, G., & Heckman, T. M. 2009, *MNRAS*, **397**, 135
- Kauffmann, G., Heckman, T. M., Tremonti, C., et al. 2003, *MNRAS*, **346**, 1055
- Kewley, L. J., Dopita, M. A., Sutherland, R. S., Heisler, C. A., & Trevena, J. 2001, *ApJ*, **556**, 121
- Kewley, L. J., Groves, B., Kauffmann, G., & Heckman, T. 2006, *MNRAS*, **372**, 961
- Kewley, L. J., Nicholls, D. C., Sutherland, R., et al. 2019, *ApJ*, **880**, 16
- Kewley, L. J., Nicholls, D. C., & Sutherland, R. S. 2019, *ARA&A*, **57**, 511
- Kewley, L. J., Maier, C., Yabe, K., et al. 2013a, *ApJ*, **774**, 10
- Kovacevic, J., Popovic, L. C., & Dimitrijevic, M. S. 2010, *ApJS*, **189**, 15
- Kuraszkiewicz, J., Wilkes, B. J., Atanas, A., et al. 2021, *ApJ*, **913**, 134
- Netzer, H. 2015, *ARA&A*, **53**, 365
- Proxauf, B., Ottl, S., & Kimeswenger, S. 2014, *A&A*, **561**, 10
- Ramos, A. C., Levenson, N. A., Alonso-Herrero, A., et al. 2011, *ApJ*, **731**, 92
- Richards, G. T., Fan, X. H., Newberg, H. J., et al. 2002, *AJ*, **123**, 2945
- Ross, N. P., Myers, A. D., Sheldon, E. S., et al. 2012, *ApJS*, **199**, 3
- Sanders, R. L., Shapley, A. E., Kriek, M., et al. 2016, *ApJ*, **816**, 23
- Shen, Y., Richards, G. T., Strauss, M. A., et al. 2011, *ApJS*, **194**, 45
- Sun, A. L., Greene, J. E., & Zakamska, N. L. 2017, *ApJ*, **835**, 222
- Zakamska, N. L., Strauss, M. A., Krolik, J. H., et al. 2003, *AJ*, **126**, 2125
- Zhang, X. G. 2021a, *ApJ*, **909**, 16
- Zhang, X. G. 2021b, *MNRAS*, **502**, 2508
- Zhang, X. G. 2022, *MNRAS*, **509**, 4626
- Zhang, X. G., & Feng, L. L. 2016, *MNRAS*, **457**, 3878
- Zhang, X. G., & Feng, L. L. 2017, *MNRAS*, **468**, 620
- Zhang, X. G., Feng, Y., Chen, H., & Yuan, Q. 2020, *ApJ*, **905**, 97